atmosphere

MDPI

Article

Numerical Analysis of the Effects of Different Window-Opening Strategies on the Indoor Pollutant Dispersion in Street-Facing Buildings

Yongjia Wu [1,2], Yilian Ouyang [1], Tianhao Shi [1,3,*], Zhiyong Li [1] and Tingzhen Ming [1,2,*]

[1] School of Civil Engineering and Architecture, Wuhan University of Technology, Wuhan 430070, China; oyyl@whut.edu.cn (Y.O.)
[2] Sanya Science and Education Innovation Park, Wuhan University of Technology, Sanya 572004, China
[3] CITIC General Institute of Architectural Design and Research Co., Ltd., Wuhan 430014, China
* Correspondence: thshi@whut.edu.cn (T.S.); tzming@whut.edu.cn (T.M.)

Abstract: The idling of automobiles at street intersections can lead to pollutant accumulation which impacts the health of residents in street-facing buildings. Previous research focused on pollutant dispersion within street canyons and did not consider the coupling of indoor and outdoor pollutants. This paper employs the computational fluid dynamics (CFD) method to simulate the dispersion characteristics of vehicle emission pollutants in street canyons, primarily investigating the indoor and outdoor pollutant dispersion patterns under various window opening configurations (single-sided ventilation, corner ventilation, and different positions of the glass under corner ventilation). Additionally, the study considers the impacts of the aspect ratio and ambient wind speed. Studies have shown that corner ventilation is effective in reducing indoor pollutant levels. When the two window glass positions are far away from the center of the intersection, the average CO mass fraction in the single-sided ventilation room is reduced by 87.1%. The average indoor CO mass fraction on the leeward side decreases with the increasing wind speed and aspect ratio. At a wind speed of 8 m/s, the average indoor CO mass fraction on the leeward side decreases to 2.45×10^{-8}. At an aspect ratio of 2, the indoor CO mass fraction on the leeward side decreases with increasing floors before stabilizing at approximately 4.77×10^{-9}. This study suggests optimal window opening strategies to reduce indoor pollutant levels in street-facing buildings at street intersections, offering guidance to indoor residents on window ventilation practices.

Keywords: street intersections; computational fluid dynamics; street canyon; window opening; natural ventilation

check for updates

Citation: Wu, Y.; Ouyang, Y.; Shi, T.; Li, Z.; Ming, T. Numerical Analysis of the Effects of Different Window-Opening Strategies on the Indoor Pollutant Dispersion in Street-Facing Buildings. *Atmosphere* **2024**, *15*, 724. https://doi.org/10.3390/atmos15060724

Academic Editor: Prashant Kumar

Received: 10 April 2024
Revised: 23 May 2024
Accepted: 31 May 2024
Published: 17 June 2024

Copyright: © 2024 by the authors. Licensee MDPI, Basel, Switzerland. This article is an open access article distributed under the terms and conditions of the Creative Commons Attribution (CC BY) license (https://creativecommons.org/licenses/by/4.0/).

1. Introduction

The accelerating process of urbanization and the increasing demand for transportation have led to the deterioration of urban air quality, emerging as a critical urban environmental issue [1]. Apart from adversely affecting pedestrians outdoors, pollutants infiltrate indoor spaces through various pathways such as doors, windows, ventilation ducts, and building cracks, posing risks to indoor residents [2]. Considering that individuals spend approximately 90% of their time indoors, buildings offer limited protection against ambient air pollution [3]. Urban residents residing in street-front buildings encounter substantial exposure to vehicle pollutants, which can significantly impact human health and the overall living environment, particularly causing severe respiratory illnesses among vulnerable populations such as the elderly and children. Conventional air-conditioning systems often fail to supply fresh air adequately, necessitating natural ventilation in some buildings. Additionally, stores along streets must remain open for business purposes, and residential buildings and schools require periodic window openings to mitigate indoor air pollution [4]. Existing research and practical applications indicate that natural ventilation remains an

effective strategy under certain conditions, especially where resources are limited or air conditioning systems are impractical. In addition to energy savings, natural ventilation can remove pollutants and heat very effectively from an indoor space and minimize building-related illnesses. But, the natural ventilation effect is greatly affected by external climate conditions (such as wind speed, wind direction, and temperature differences), and it is difficult to ensure a stable ventilation effect. To examine the dispersion patterns of pollutants in urban settings under natural ventilation, researchers' studies have focused on analyzing pollutant dispersion in street canyons through CFD simulations [5–9], wind/water tunnel experiments [2,10–12], and field measurements [13–15].

The primary source of pollutant exposure within street canyons stems from vehicle emissions, which vary across vehicle models and emission levels under distinct driving conditions. Motor vehicles often idle for more than 25% of their operational time [16], entering a specific idling state while parked and waiting. Ineffective combustion during engine idling leads to increased pollutant emissions. Due to the inability of pollutants to disperse through the wake produced by moving vehicles [17,18], the impact on street canyons and buildings facing streets is more pronounced during idle states compared to motion.

Key factors impacting the dispersion of airborne pollutants within a street canyon encompass the street's aspect ratio [19] (expressed as the building height/street width, H/W) and the building density. Moreover, numerous other elements, including the morphological structure of the street canyon [20,21], the encompassing elevated building designs [22–24], wind traps [25–27], vegetation [28,29], and billboard placement [30], alongside ambient conditions like wind patterns [31] and solar radiation [32,33], markedly affect the airflow patterns within a street canyon.

In addition to the factors mentioned earlier, various types of street canyons significantly influence pollutant dispersion. Intersections, compared to regular street canyon roads, exhibit more intricate inner flow patterns. Vehicles often idle at intersections due to traffic light control, emitting higher levels of pollutants, leading to localized pollutant concentrations being higher than those observed in normal street canyons. Surveys indicate that intersections were the areas within cities with the most severe pollutants emissions, particularly CO [34]. Scholars have extensively investigated characteristic flow patterns within street canyons at intersections. Scaperdas et al. [35] found that the detected CO_2 concentrations exhibited fluctuations of up to 80% in response to varying wind directions. Li et al. [36] found the lowest PM concentrations above the sidewalk at a breathing height of 1.5 m above the ground and the least PM concentrations on the roofs of all building surfaces. Hassan et al. [37] highlighted the significant role of three-dimensional interconnections between dominant canyon vortices and the flow at roof level in determining the pollutant concentrations on the windward wall. Guo et al. [34] demonstrated that three-way intersections exhibited higher ventilation efficiency compared to other intersection types at similar average wind speeds. Moreover, they noted a positive correlation between the angle between streets and increased ventilation efficiency. He et al. [38] found that the flow field is significantly impacted by both the prevailing wind direction and the orientation of the adjacent roadway sections. However, solely studying the dispersion of pollutants within the street canyon at intersections is inadequate, overlooking the potential harm posed to indoor occupants of street-facing buildings due to the accumulation of substantial pollutant concentrations at these junctions.

Many urban buildings rely on natural ventilation to mitigate indoor air pollution. The microclimate of urban street canyons, including factors like wind speed, surface temperature differences, and pollutant concentrations, significantly affects indoor environmental quality. Insufficient ventilation rates and excessive infiltrations of outdoor pollutants represent two primary risks associated with natural ventilation in urban buildings. Previous findings indicate that planning urban street canyons and designing building envelopes play pivotal roles in controlling indoor environmental quality and optimizing the utilization of natural ventilation in buildings [4]. Yang et al. [39] observed that alterations in window

opening rates (WOPs) affected the pressure distribution around a downstream building. Additionally, an increase in WOPs corresponded to heightened indoor ventilation within the downstream building. Gao et al. [40] conducted CFD simulations to explore optimal and suboptimal opening configurations, diverse building orientations, and varying wind conditions using different window types. Hu et al. [5] found that cross-ventilation can significantly improve the air change rate and pollutant dilution in residential buildings under isothermal conditions. Peren et al. [41] observed that vertical variations in outlet opening locations minimally affect the volumetric flow rate. Prakash et al. [42] found that a 50% increase in the percentage of low temperatures for the optimal window opening position compared to the least optimal position. Additionally, PMV and PPD decreased by 0.12% and 3.51%, respectively. Ongoing investigations into coupled indoor and outdoor pollutants primarily focus on single-sided and through ventilation. Nevertheless, it is important to note that corner ventilation, by adeptly harnessing wind direction and velocity, fosters a more uniform and sustained indoor airflow.

In general, few studies have been conducted to date on the dispersion of pollutants in the interiors of street-facing buildings at intersections. This paper is written to fill a gap in the research in the field. Unlike previous efforts, this paper conducts CFD simulations and experimental validations to study the interaction between indoor and outdoor pollutants in buildings situated at a typical intersection street canyons, aiming at clarifying the genuine effects of window-opening methods on indoor environments. Building upon earlier research, this work aims to more accurately predict the impact of street canyon vehicles on the indoor environments of street-facing buildings, aiming to provide indoor residents with window openings that are conducive to maintaining a healthy indoor environment.

2. CFD Methodology

2.1. Geometric Model

Street canyons encompass urban streets and adjacent buildings. This paper predominantly focuses on the indoor–outdoor interaction of pollutants and does not carry out in-depth research on the complex street canyon structure. The study selected an optimal cross-street canyon (H/W = 1) featuring low-height residential buildings on both sides. It evaluates the impact of carbon monoxide emissions from numerous idle automobiles waiting at traffic lights on people on sidewalks and indoor residents. Additionally, the analysis includes assessing the effects of various window openings on indoor pollutant dispersion in a corner-ventilated state.

This paper presents an idealized model of a four-lane intersection street canyon, simulating these conditions under perpendicular wind conditions. As depicted in Figure 1, both the building height (in the *Z*-axis direction) and the street width measure 24 m. The road aligned along the *X*-axis serves as the main road, whereas the road aligned along the *Y*-axis functions as the secondary road. The dimensions of the rooms and windows are referenced from Hang et al. [43]. Model dimensions are shown in Table 1. Eight rooms, each measuring 5.7 m in length, 4 m in width, and 2.7 m in height, were arranged at the corners of the building. Additionally, these rooms had a wall thickness of 0.3 m. The first floor includes two doors (5.7 m × 2 m and 4 m × 2 m), while floors two to eight feature two windows (4 m × 1 m). The street setup includes a 4 m wide sidewalk and a 16 m wide driveway, with the inlet and outlet situated 24 m away from the upstream and downstream buildings, respectively. The computational domain's top is positioned 24 m from the building. The model's symmetry around the *X* and *Y* axes considers rooms only in buildings 1 and 2. This study adopts the nomenclature L and W as prefixes, designating room floors as suffixes to name all rooms situated on the windward and leeward sides. Rooms on the windward side are denoted as W1–W8, while those on the leeward side are represented as L1–L8. The study comprises nine cases exploring varied window-glazing positions' impact on indoor pollutant concentrations in street-facing buildings. Cases 1, 2, and 3 investigate the diffusion of indoor and outdoor pollutants in the pivotal building for three window positions on Road 1: away from the intersection, in the center, and near the

intersection. Cases a, b, and c analyze the diffusion of indoor and outdoor pollutants in the crucial building for three glazing positions on Road 2: away from the intersection, in the center, and close to the intersection. Figure 2 and Table 2 illustrate window-opening methods and case settings, with blue representing glass in the visual representations.

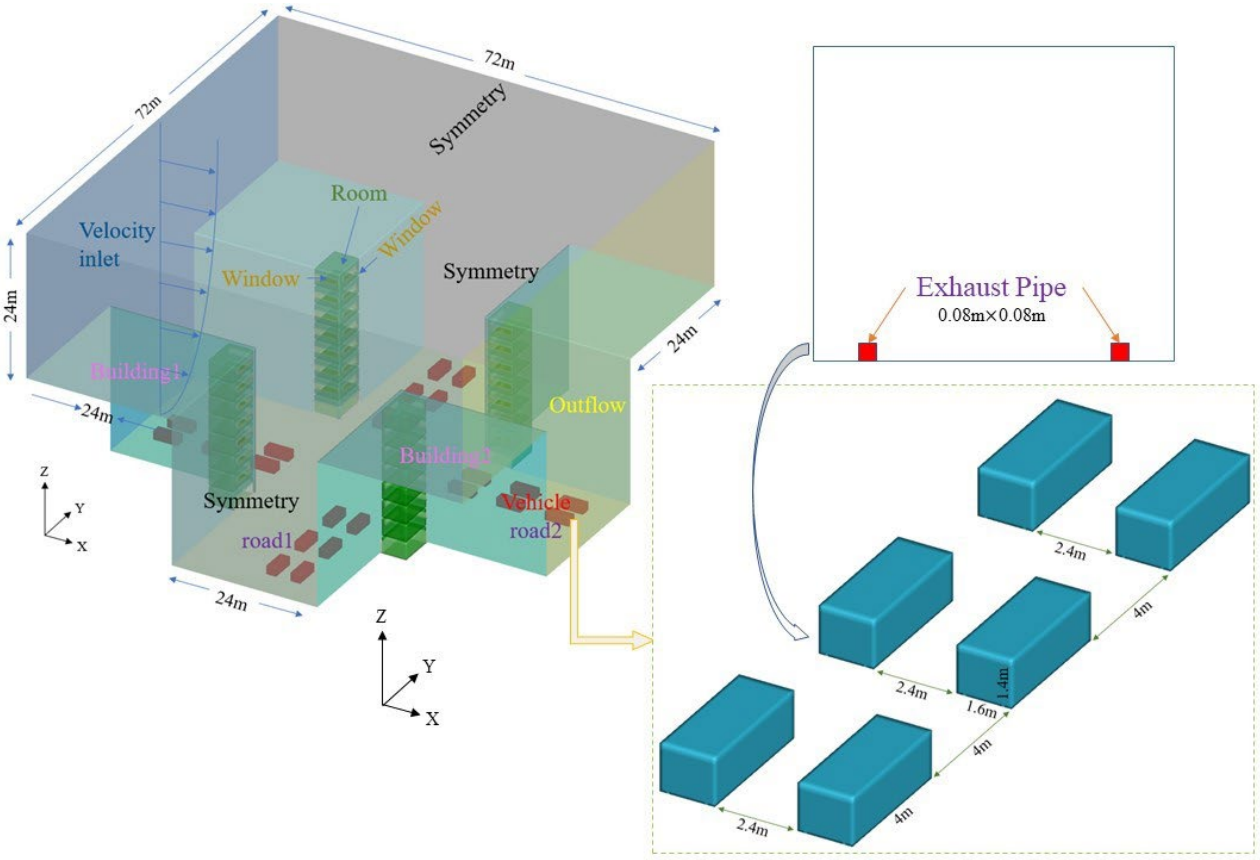

Figure 1. The geometric model.

Table 1. The dimensions of the room models.

Name	Size
Room	5.7 m × 4 m × 2.7 m
Window	4 m × 1 m
Door	5.7 m × 2 m
Building	24 m
Car	4 m × 1.6 m × 1.4 m
Exhaust pipe	0.08 m × 0.08 m

Figure 2. The window-opening methods.

Table 2. Cases and window-opening settings.

Case	Opening of Windows on Road 1	Opening of Windows on Road 2
Case 1.a	Away from crossroads	Away from crossroads
Case 1.b	Away from crossroads	In the center
Case 1.c	Away from crossroads	Near crossroads
Case 2.a	In the center	Away from crossroads
Case 2.b	In the center	In the center
Case 2.c	In the center	Near crossroads
Case 3.a	Near crossroads	Away from crossroads
Case 3.b	Near crossroads	In the center
Case 3.c	Near crossroads	Near crossroads

City roads accommodate a variety of vehicles with diverse forms and exhaust systems, including minivans, SUVs, and buses. To streamline calculations, a simplified car model is employed. The vehicle is situated on a plane at a height of 0.4 m, measuring 4 m × 1.6 m × 1.4 m, and features two exhaust vents, each sized 0.08 m × 0.08 m. Dynamic pollutant dispersion analysis focused solely on carbon monoxide (CO) emissions from the vehicle. The investigation assumed a pollutant concentration of 10 ppm at the exhaust outlet and an exit velocity of 5.5 m/s, excluding the consideration of temperature effects.

2.2. Mathematical Model

Three common CFD approaches, namely Navier–Stokes (RANS), Large Eddy Simulation (LES), and Direct Numerical Simulation (DNS), are employed for pollutant simulation in turbulence. While LES and DNS offer precise results by computing the flow field in time and space, they demand increased computational time and stricter equipment performance compared to the RANS approach. DNS calculates all turbulence scales but is unsuitable for high Reynolds number street canyon flows, while LES resolves large-scale energy-containing turbulent fields. RANS proves effective in predicting street-scale turbulence without extensive computational demands or complex meshing. Hence, the RANS turbulence model, specifically the RNG k-ε model, is utilized in this study for its successful application in previous research concerning turbulence and pollutant dispersion in street canyons. Consequently, this paper employs the RNG k-ε turbulence model combined with the standing wall function to simulate a steady-state isothermal street canyon flow using ANSYS Fluent 19.0. The governing equations of mass, momentum, turbulent kinetic energy, and the dissipation rate are as follows.

The continuity equation:

$$\frac{\partial u_i}{\partial x_i} = 0 \tag{1}$$

Momentum equation:

$$U_i \frac{\partial U_i}{\partial x_j} = -\frac{1}{\rho}\frac{\partial p}{\partial x_i} + \frac{\partial}{\partial x_j}\left(v\left(\frac{\partial U_i}{\partial x_j} + \frac{\partial U_j}{\partial x_i}\right) - u_i^{'}u_j^{'}\right) + \left(\frac{\rho - \rho_0}{\rho_0}\right)g_i \tag{2}$$

$$u_i^{'}u_j^{'} = v_t\left(\frac{\partial U_i}{\partial x_j} + \frac{\partial U_j}{\partial x_i}\right) - \frac{2}{3}\delta_{ij}k \tag{3}$$

Energy Equation:

$$U_j \frac{\partial T}{\partial x_j} = \alpha \frac{\partial^2 T}{\partial x_i \partial x_j} - \frac{\partial}{\partial x_j}\left(T^{'}u_j\right) \tag{4}$$

Turbulent kinetic energy k:

$$U_j \frac{\partial k}{\partial x_i} = \frac{\partial}{\partial x_j}\left[\left(v + \frac{v_t}{\sigma_k}\right)\frac{\partial k}{\partial x_j}\right] + G - \varepsilon \tag{5}$$

$$v_t = C_\mu \frac{k^2}{\varepsilon} \tag{6}$$

Turbulent kinetic energy dissipation rate:

$$U_i \frac{\partial \varepsilon}{\partial x_i} = \frac{\partial}{\partial x_j}\left[\left(v + \frac{v_t}{\sigma_\varepsilon}\right)\frac{\partial \varepsilon}{\partial x_j}\right] + C_{1\varepsilon}\frac{\varepsilon}{k}G - \left[C_{2\varepsilon} + \frac{C_\mu \rho \eta^3 \left(1 - \frac{\eta}{\eta_0}\right)}{1 + \beta\eta^3}\right]\frac{\varepsilon^3}{k} \tag{7}$$

where ρ denotes the air density, v denotes the kinematic viscosity, P denotes the air pressure, δ_{ij} denotes the Kronecker delta, k and ε denote the turbulence kinetic energy and turbulence dissipation rate, respectively, C_μ, $C_{1\varepsilon}$, and $C_{2\varepsilon}$ denote empirical values taken as 0.09, 1.44, and 1.92, respectively, $u_i^{'}u_j^{'}$ denotes the Reynolds stress term, and σ_k and σ_ε denote the k and ε corresponding turbulence Prandtl numbers, which are taken as 1.0 and 1.3, respectively. $\eta = \left(\frac{k}{\varepsilon}\right)\left(\frac{G}{v_t}\right)$ 0.5, $\beta = 0.012, \eta_0 = 4.38$.

Species transportation equations:

$$u_j \frac{\partial c}{\partial x_j} = \frac{\partial}{\partial x_j}\left(K_c \frac{\partial c}{\partial x_j}\right) + S_c \tag{8}$$

where C denotes the pollutant concentration (kg/m^3), S_c denotes the pollutant emission rate (kg/m^{3}s), K_c denotes the turbulent diffusion coefficient of pollutants, $K_c = v_t / Sc_t$, which was analyzed by Hang et al. [44], and Sc_t was taken as 0.7.

2.3. Boundary Conditions

In Figure 1, the boundary conditions for the computational domain are illustrated. These include a no-slip condition implemented with a standard wall function on the near-wall surface. A gradient ambient wind condition is set at the inlet of the domain, which is perpendicular to the street canyon. The outlet boundary condition is set as a pressure outlet, and the symmetry boundary conditions are applied to the top and two sides of the computational domain. Additionally, zero normal gradient conditions are set for the top, sides, and exit of the computational domain. The exhaust port at the car's rear end is configured as a velocity inlet. For analysis simplification, user-defined functions are utilized to set the velocity, turbulent kinetic energy (TKE), and dissipation rate at the computational domain's inlet, as expressed in the subsequent equation:

$$U_z = U_{ref}\left(\frac{z - 20}{z_{ref}}\right)^{\alpha} \tag{9}$$

$$k = \frac{\left(U^*\right)^2}{\sqrt{C_\mu}} \tag{10}$$

$$\varepsilon = \frac{\left(U^*\right)^3}{\kappa z} \tag{11}$$

where the reference velocity U_{ref} = 2 m/s, the reference height z_{ref} = 24 m, α denotes the ground roughness index, which is taken as 0.2 after the study by Chen [45] and others, U^* denotes the friction velocity [46], and the von Karman constant κ = 0.42.

Ensuring Reynolds number independence necessitates Re to be significantly larger than 3.3×10^4 [47]. For this study, the reference height of the building (H = 24 m) yields a calculated reference Reynolds number of approximately 2,651,934, surpassing 3.3×10^4 by a substantial margin, thereby confirming the independence of the Reynolds number.

2.4. Mesh Generation and Sensitivity Analysis

Mesh quality significantly influences the accuracy of CFD simulation results. Unstructured meshes, despite their slow generation and typical poor quality, differ from structured meshes known for their straightforward construction and computational efficiency. The study employs a high-quality regular geometric model, depicted in Figure 3. Near the wall, a minimum grid size of 0.02 m ensures a y+ value of about 20 at the boundary. Meanwhile, within the street canyon interior (excluding the vehicle), a larger grid size of $\Delta x \times \Delta y = 0.3\ m \times 0.3\ m$ is utilized. The mesh expansion ratio is set at 1.02, resulting in a total of 12,370,808 generated meshes. Additionally, a grid size of $\Delta x \times \Delta y = 0.2\ m \times 0.2\ m$ is applied above the travel lane, near the vehicle.

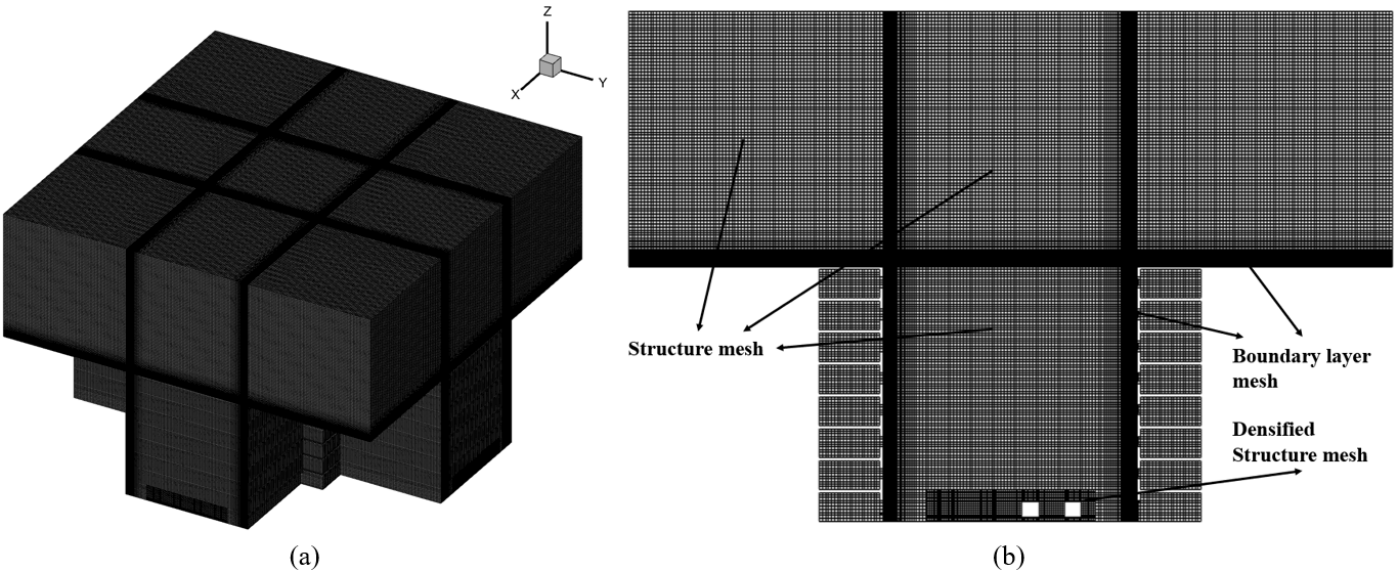

Figure 3. A schematic diagram of the mesh: (**a**) the mesh of the calculation domain; and (**b**) the mesh of the cross-section.

The discretization of convective terms utilizes a second-order windward scheme. Additionally, the interpolation of the gradient term is managed using the Green-Gaussian nodal scheme. The SIMPLE algorithm is employed for the numerical calculation, striving for convergence with criteria set at maximum residuals of less than 1×10^{-5} for the concentration, mass, and momentum, alongside values below 1×10^{-8} for the energy equation.

To assess the mesh independence, this study evaluated three different mesh systems—8,853,672, 13,483,496 and 19,251,664, representing varying accuracies (rough, moderate, and fine) under consistent operating conditions (U_{ref} = 2 m/s, stationary vehicle). The investigation focused on the Z = 2 m and Y = 0 line to compare the velocity and mass fraction of CO across the three mesh systems as shown in Figure 4. Figure 5 illustrates that the maximum errors in the velocity and mass fraction of CO across the three grid systems remain below 5%, falling within an acceptable range. Despite a notable error at grid number 8,853,672, there was no significant variation in the velocity and mass fraction of CO observed when increasing the grid number from 13,483,496 to 19,251,664, demonstrating grid independence. As a baseline, this paper adopts the intermediate value of 13,483,496, adjusting the number of meshes in other models relative to this standard.

Figure 4. A sketch of the street intersection model.

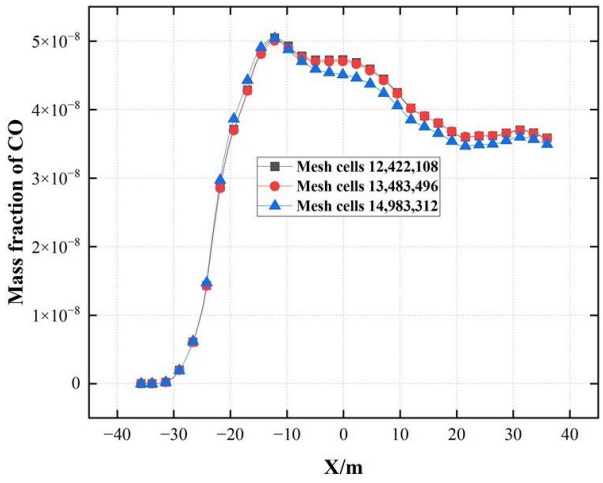

(a)

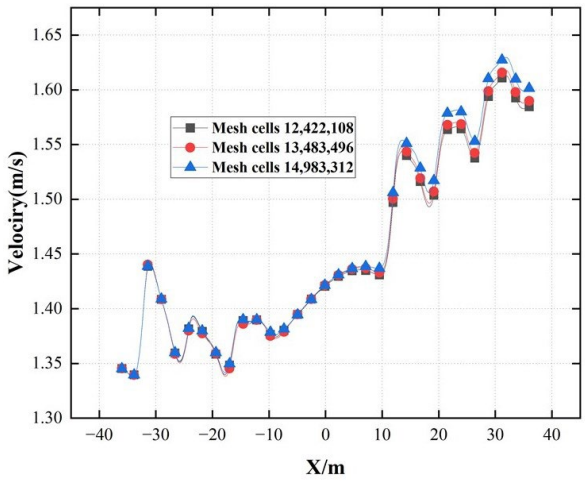

(b)

Figure 5. The grid independence test results: (**a**) the mass fraction of CO, and (**b**) the wind velocity.

2.5. Model Validation

2.5.1. For Flow Field

To gauge the accuracy of physical and mathematical models for a regular street intersection (aspect ratio of 1), Janour's [48] wind tunnel experimental data are used for validation in this study. The wind tunnel, featuring a 1.5 m × 1.5 m cross-section, conducted measurements at a distance of 25.5 m from the entrance. Reference velocity (U_{ref}) measurements were obtained using a 2D fiber-optic laser Doppler anemometer (DANTEC) equipped with a velocity sensor. Measurements of wind speed variation along the Z-axis were taken at the specific coordinates of X/H = 0 and Y/H = 1.5. The exact geometric model and boundary conditions were replicated for numerical simulations utilizing the data from the reference Yassin's paper [49]. Pollutant emissions are depicted by a continuous line source of pollutants on the ground, aligned parallel to the y-axis. CO_2 is chosen as the tracer gas for the study. The length of the line source is 0.5 m. The characteristic wind speed is represented by U_{ref} = 2 m/s. The CO_2 flow is uniformly discharged at a speed of Q_S = 40 L/h. Data on calculated and measured normalized horizontal velocity and concentration ratios at various locations in standard street intersections are presented. The concentration is expressed in a dimensionless form as $K = CU_H HL_Q/Q$ where C represents the CO_2 concentration, U_H represents the wind speed at the height of the street canyon, H denotes the building height, L_Q signifies the line source length, and Q denotes the source intensity. Figure 6 presents a comparison of the results, illustrating that the data derived from numerical simulations in this paper moderately align with the wind tunnel test data. Despite some deviations, the errors observed remain within an acceptable range.

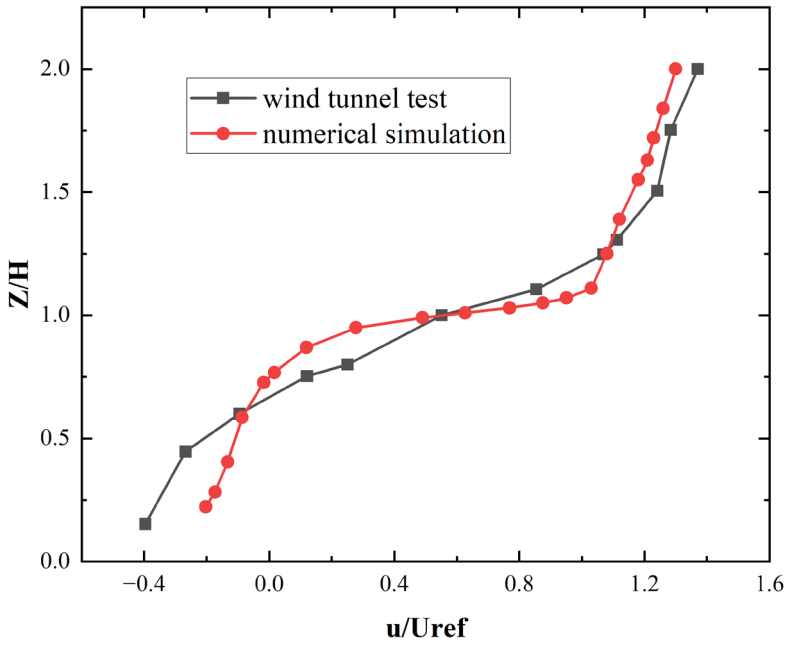

Figure 6. A comparison of the simulation results in this paper and Yassin's [49] results.

2.5.2. For Vehicle Exhaust Jets

Following the verification of the velocity field, the analysis extended to verify the concentration field by referencing Meroney's [50] wind tunnel test data. Experiments were conducted in the Atmospheric Boundary Layer Wind Tunnel (BLASIUS) at the Institute of Meteorology of the University of Hamburg to investigate the dispersion of vehicle exhaust gases in urban street canyons under neutral conditions, focusing on the influence of street geometry on pollution dispersion. Wind speed was continuously recorded using a Prandtl pitot-static tube and a conventional hot-film, Thermal Systems Inc. (TSI) Modle 1210-20. A DC motor, equipped with a thyristor-based control system, regulates test-section wind speeds ranging from 0 to 15 m/s. The effective working section measures 1 m in height,

1.5 m in width, and 4 m in length, preceded by a 7.5 m long development section downstream of the boundary layer stimulation system. Based on wind tunnel experimental data, an idealized street canyon model with an aspect ratio of 1 was constructed, with the ambient wind blowing perpendicular to the street canyon. The model featured a building height of 0.06 m and emissions of ethane and air at rates of Q_e = 1.4 l/h and Q_a = 100 L/h, respectively, with ethane serving as the tracer gas. The dimensionless concentration of K (ethane) was determined by quantifying U_{ref} (free wind speed, 1 m/s) measured at a height of 0.65 m above the street level. Figure 7 presents comparisons between the numerical simulations and experimental data, showcasing consistent trend distributions of the dimensionless concentration of pollutants on the windward and leeward sides. This demonstrates the effectiveness of the developed model and computational simulation method in analyzing the pollutant concentration field within the street canyon.

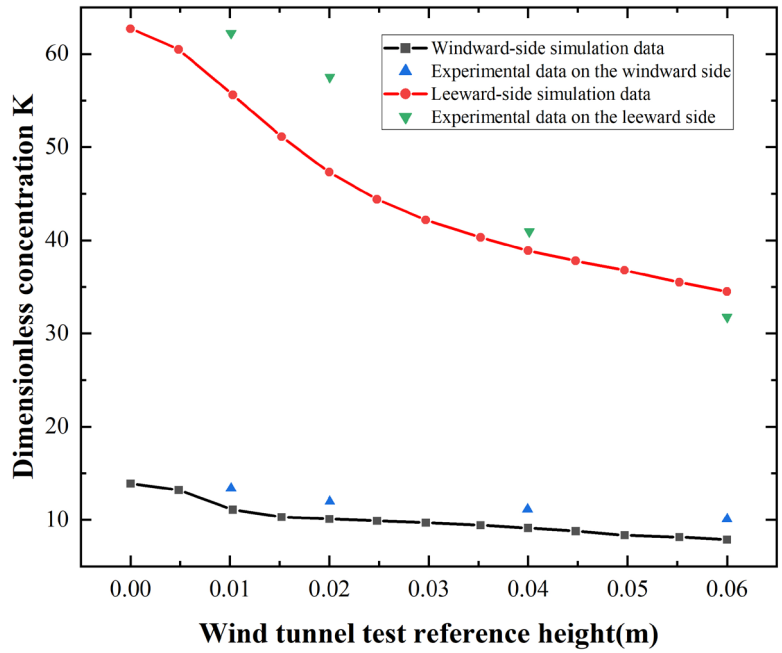

Figure 7. A comparison of the simulation results with wind tunnel test results [50].

2.5.3. For the Verification of Indoor–Outdoor Airflow Coupling

In order to validate the indoor–outdoor coupling, Jiang's wind tunnel experimental data [51] is utilized in this paper for verification. The experiments were carried out in the wind tunnel at Cardiff University, which has an area of 2 m × 2 m and a height of 1 m. The instrument used to measure the velocity distribution around and inside the model is a one-dimensional LDA system commercially produced by Dantec. The building model is square, with a height of H = 250 mm and an opening of 84 mm × 125 mm. The incoming winds were oriented perpendicular to the axis of the building. The values are taken at different locations on the center plane of the building (Y = 0) for comparison. Figure 8 shows the building model for the wind tunnel test. The numerical simulation graphs are compared with the experimental results as shown in Figure 9, and the trends are found to be largely consistent, with deviations falling within acceptable limits. The reason for these discrepancies may be due to the measurement error of the experimental instrument or the computational inaccuracies in the numerical model. Overall, the turbulence model chosen in this paper demonstrates an effective simulation of indoor and outdoor air flow.

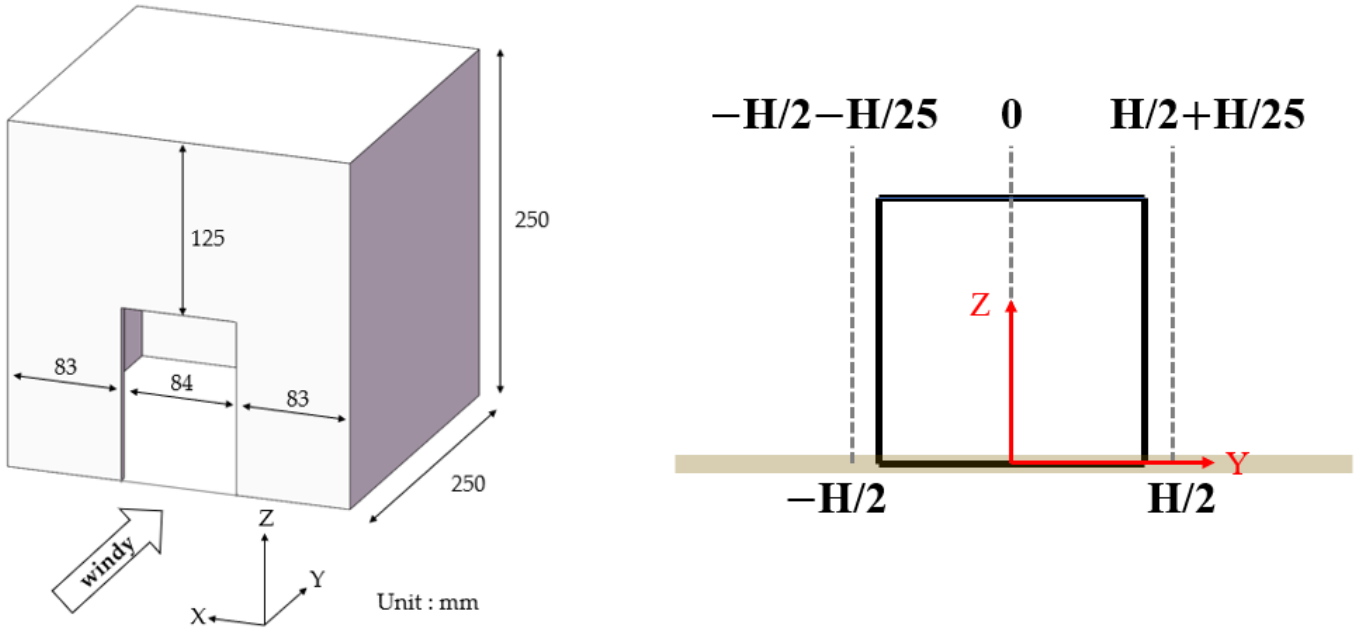

Figure 8. The building model and the location of the speed measurement points [51].

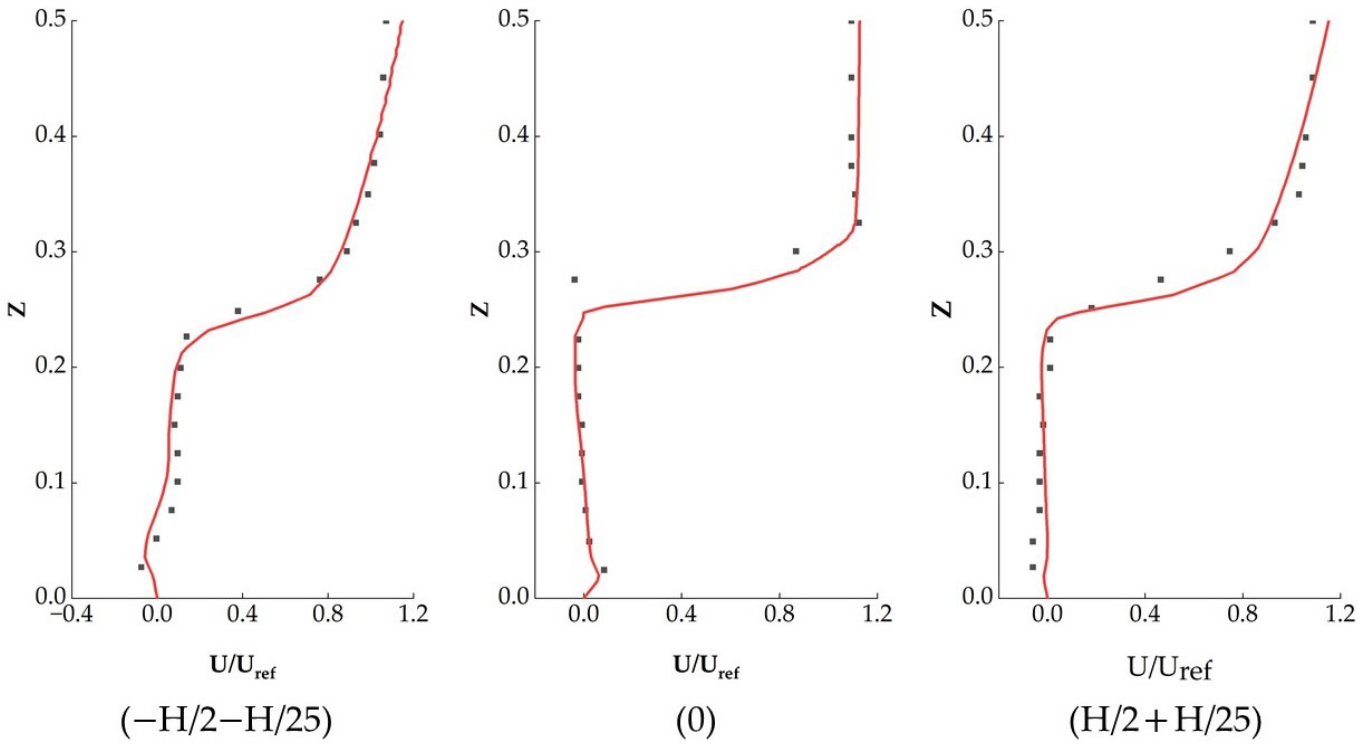

Figure 9. The vertical distribution of the velocity (solid lines are simulation results, black dots are experimental results) [51].

3. Results

3.1. Characteristics of Indoor Pollutant Diffusion under Different Window-Opening Methods

The configuration of a building's exterior windows and their placement significantly influences indoor airflow patterns and pollutant dispersion. This section examines the impact of two common window configurations—single-sided ventilation (SSV, opening in the same façade) and corner ventilation (CV, opening in the perpendicular façades)—as well as diverse window locations in street-facing buildings on the indoor and outdoor transport

of pollutants within rooms situated in street-facing buildings at intersections. Further investigation was conducted on CV to assess the impact of full-end sliding windows in rooms of buildings facing street intersections on indoor and outdoor pollutant transport at various positions. Subsequently, a cross-section at Y = −14.3 (positioned at the window's center on Road 1) was taken for each scenario and examined, as depicted in Figure 10. The indoor mass fraction of CO in individual rooms was then compared to the average indoor mass fraction of CO. Here, the indoor mass fraction of CO represents the mean mass fraction of CO at a height of 1.7 m within each room, while the average indoor mass fraction of CO signifies the mean mass fraction of CO across all individual rooms within the building.

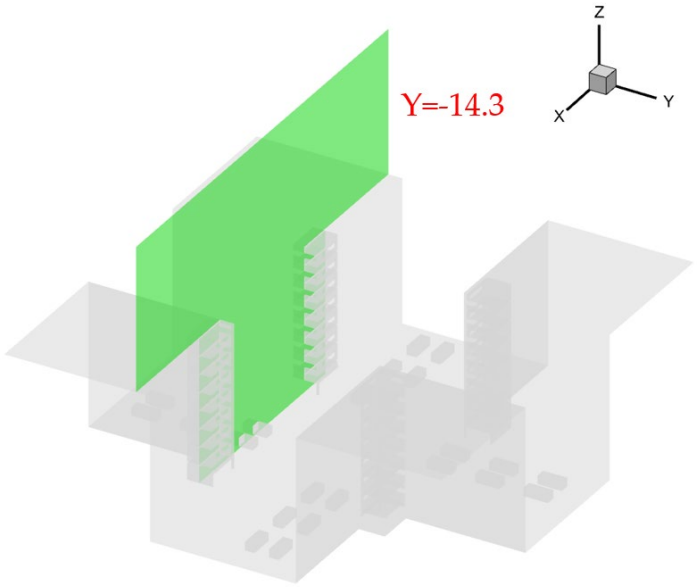

Figure 10. Section location Y = −14.3 m is located in the center of the window on Road 1.

3.1.1. Effects of Corner and Unidirectional Ventilation on Indoor–Outdoor Pollutant Coupling at Intersections

Natural ventilation prevails in traditional buildings, featuring window openings categorized into through ventilation, CV, and SSV. A limitation of penetration ventilation is its inability to control airflow direction, leading to potential unevenness in airflow distribution. CV, by leveraging wind direction and speed through building corners, ensures a more uniform and continuous airflow. This approach has garnered increasing attention in recent years [41,42]. In this section focusing on intersections, two types of natural ventilation are explored: SSV and CV, as shown in Figure 11. Each window has dimensions of 4 m × 1 m. Examine scenarios involving fully closed windows on Road 2 and fully open windows on Road 1 to exemplify SSV. Also, analyze scenarios with fully open windows on both Road 1 and Road 2 to illustrate corner openings.

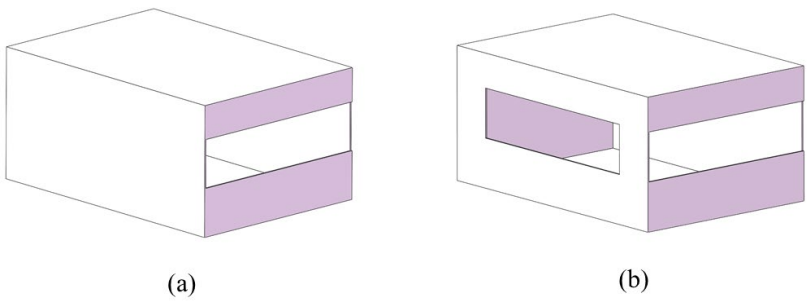

Figure 11. Window-opening methods: (**a**) SSV, and (**b**) CV.

Figure 12 displays the mass fraction of CO for each room employing SSV and CV. From the data presented, it is evident that CV exhibits a 10.7% lower average mass fraction of CO than SSV on the windward side. In the L2 room, the mass fraction of CO was 55.7% higher with CV than with SSV, whereas in the W5 and W6 rooms, it was 51% and 39.9% lower, respectively. The average mass fraction of CO in corner-ventilated rooms on the windward side was 24.5% lower at 9.19×10^{-8}, contrasting with 1.2×10^{-7} for SSV. Moreover, SSV exhibited higher indoor pollutant concentrations compared to CV across all rooms. With the exception of W1, the concentrations of indoor pollutants in the other rooms showed minimal variance, and was notably within 12.7% for CV and 15.3% for SSV.

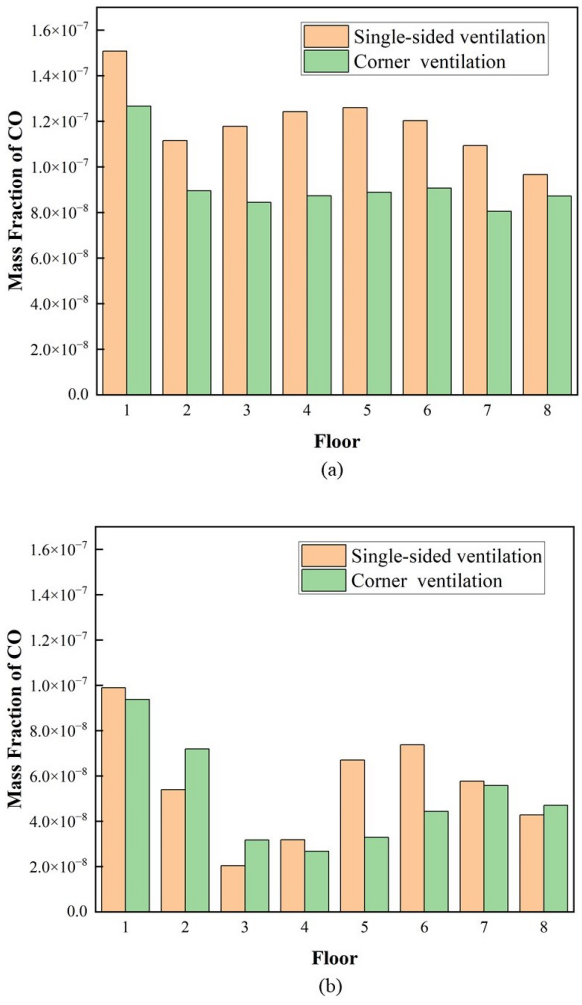

Figure 12. The indoor mass fraction of CO on the windward and leeward sides under SSV and CV: (**a**) on the leeward side, and (**b**) on the windward side.

Figure 13 depicts the indoor and outdoor mass fraction of CO distribution at Y = −14.3 (the center of the window) for both SSV and CV. The illustration demonstrates that indoor pollution concentrations with CV are notably lower on both the windward and leeward sides compared to SSV. However, there are higher concentrations observed on the lower floors of the windward side. This is due to the open window on the windward side inducing a sub-vortex at the bottom of the windward side of the street canyon, leading to pollutant accumulation and consequent higher concentrations in the nearby room. Overall, CV notably diminishes indoor pollution concentrations in buildings facing the street on both sides across most height levels.

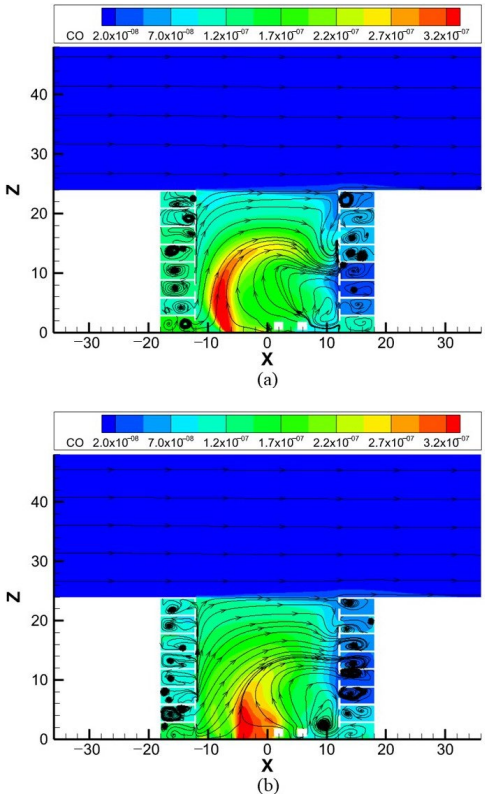

Figure 13. Indoor and outdoor mass fractions of CO for SSV and CV: (**a**) SSV and (**b**) CV.

3.1.2. The Effect of Different Locations of Glazing on the Coupling of Indoor and Outdoor Pollutants in Street-Facing Buildings at Intersections

According to the study in the previous section, CV notably amplifies the dispersion of indoor and outdoor pollutants at intersections. Thus, this section examines the impact of various positions of two windows on indoor and outdoor pollution utilizing the CV method. Illustrated in Figure 14 are three distinct glazing positions for each window: away from the intersection, centrally positioned, and near the intersection. Case 1.a, case 2.a, and case 3.a examine the dispersion of indoor and outdoor pollutants in the pivotal building with three window positions along Road 1: away from the intersection, in the center, and near the intersection. Similarly, case 1.a, case 1.b, and case 1.c investigate the spread of indoor and outdoor pollutants in the critical building with three glazing positions along Road 2: away from the intersection, in the center, and close to the intersection.

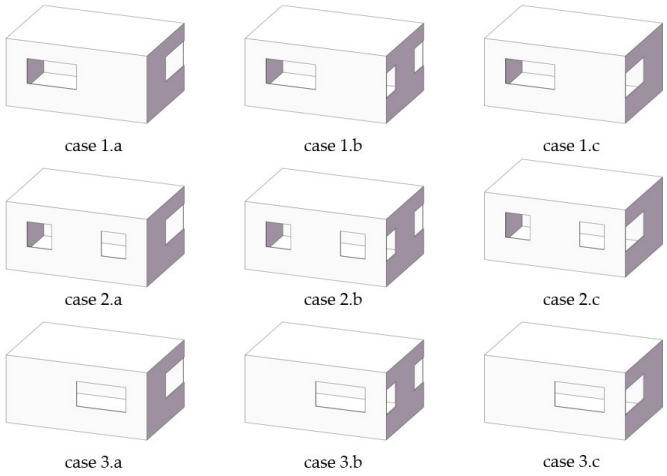

Figure 14. A 3D diagram of the different window-opening methods.

Figure 15 illustrates the indoor mass fraction of CO for each window's glass at various positions. The comparison reveals substantial variation in the data when altering the position of the glass on Road 1. Thus, the analysis focuses on maintaining the glass on Road 2 away from the intersection while positioning the glass on Road 1 away from the intersection, in the center, and close to the intersection. On the windward side, the average indoor mass fraction of CO increased by 4.98% and 5.22% for glazing positioned away from the intersection compared to the other two positions, resulting in less variability in indoor pollutant concentrations. There is a slight change in W1, with a reduction of less than 10% compared to the other two positions of the glass. W2–W5 exhibited notable changes in indoor pollutant concentrations, as the average indoor mass fraction of CO in W2–W5 decreased to 3.37×10^{-9} when the glass was positioned away from the intersection, representing a reduction of approximately 95% compared to the other two scenarios. There was an increased fluctuation in indoor pollutant concentration changes observed in W6-W8. Nevertheless, indoor pollutant concentrations were lower when Road 1 glazing was situated away from the intersection compared to the other two configurations.

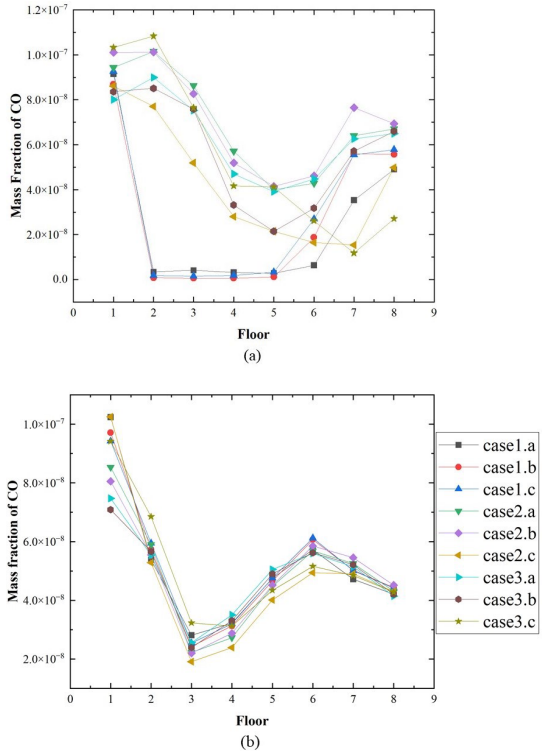

Figure 15. Mass fractions of CO in the rooms on the windward and leeward sides for different positions of the glass: (**a**) on the leeward side, and (**b**) on the windward side.

Figure 16 depicts the indoor and outdoor mass fraction of CO distributions at Y = −14.3 (the center of the window) when the window glazing on Road 2 is away from the intersection, and the position of the window glazing on Road 1 is modified. The figure illustrates that altering the position of the glass on Road 1 minimally impacts the street canyon's flow field and indoor pollutant concentrations on the leeward side, but significantly affects indoor pollutant concentrations on the windward side of the building. This occurs because the flow field in the leeward room is primarily directed from the Road 1 windows to the Road 2 windows, leading to a simpler street canyon flow structure. Conversely, the indoor flow field on the leeward side originates from the window on Road 1, generating 1–2 clockwise vortices horizontally indoors, and subsequently exiting through each of the two windows. Various glazing positions exert a more pronounced impact on indoor pollutant concentrations. In general, window-opening configurations on roads perpendicular to ambient winds markedly influenced indoor and outdoor pollution dispersions compared

to window openings on roads parallel to ambient winds. Improved indoor air quality is observed when both window panes are positioned away from the intersection.

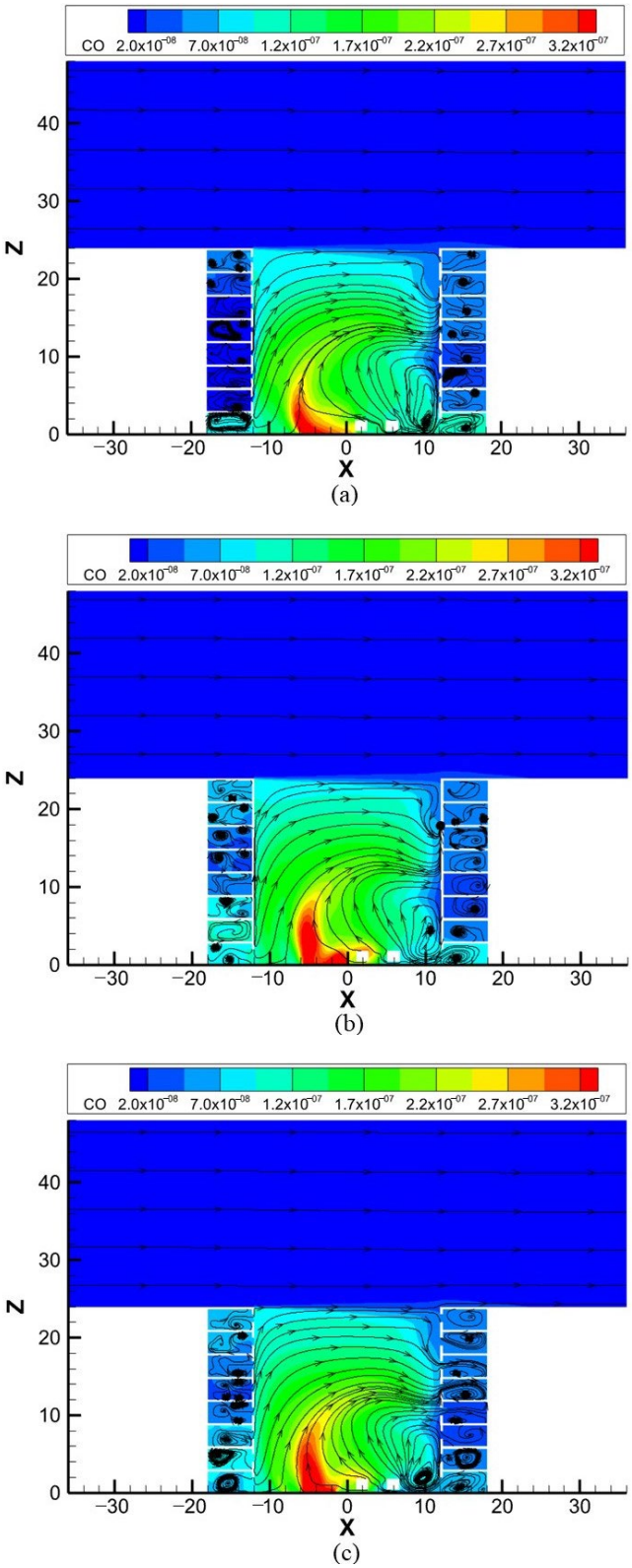

Figure 16. Indoor and outdoor mass fractions of CO for room windows on Road 2 with glazing away from the intersection: (**a**) away from the crossroads, (**b**) on the windward side, and (**c**) near the crossroads.

3.2. Effects of Ambient Wind Speed on Indoor–Outdoor Pollutant Coupling at Intersections

As the natural climate changes, so does the ambient wind speed within the city. This subsection examines the impact of three varying speeds (2 m/s, 4 m/s, and 8 m/s) on indoor and outdoor pollutant diffusion within a street-facing building featuring open windows on both adjacent walls (the data are taken from the cross-section with Y = −14.3, as shown in Figure 10). Figure 17 illustrates the indoor mass fraction of CO at three ambient wind speeds. The figure demonstrates a direct relationship: higher ambient wind speeds correspond to lower overall pollutant concentrations in the street canyon, resulting in decreased indoor pollutant concentrations as wind speed rises. Ambient wind speed minimally impacts the windward room side, while the alteration is notably significant on the leeward side. At a wind speed of 2 m/s, the leeward side's indoor environment was subpar, displaying a high indoor mass fraction of CO of 1.27×10^{-7} in W1, while the average indoor mass fraction of CO in W2-W8 stood at 3.18×10^{-8}. With increasing wind speed, the indoor mass fraction of CO declined on both sides, resulting in an average indoor mass fraction of CO of 4.58×10^{-8} and 2.45×10^{-8} on the leeward side at 4 m/s and 8 m/s, respectively.

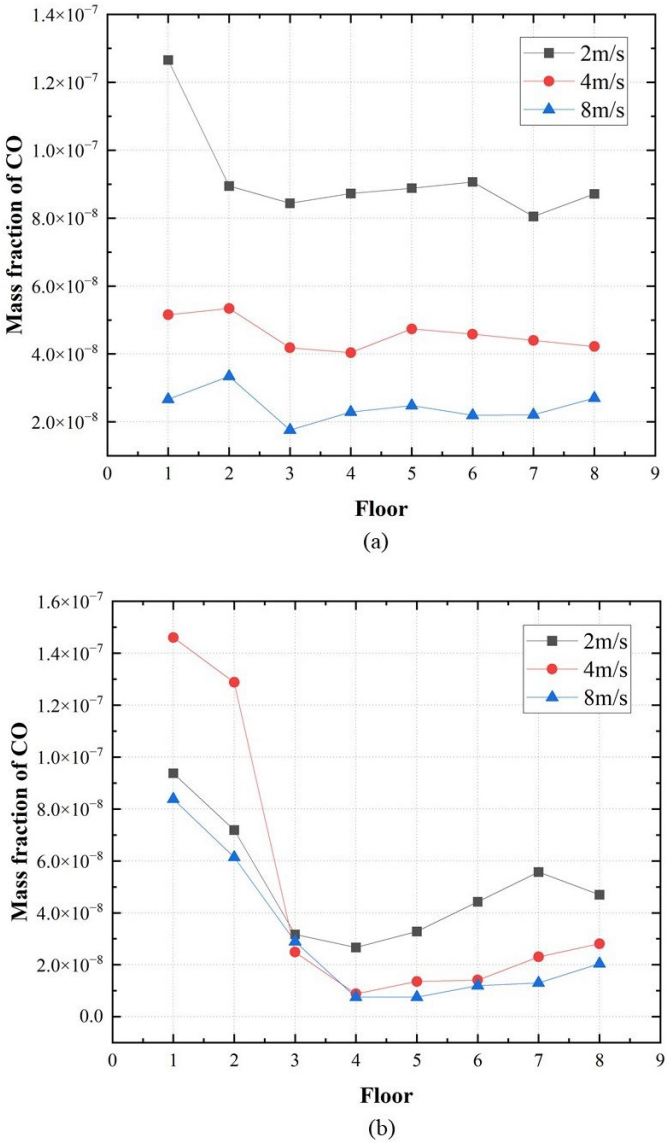

Figure 17. Indoor mass fractions of CO on the windward and leeward sides at different ambient wind speeds: (**a**) on the leeward side, and (**b**) on the windward side.

Figure 18 illustrates the distribution of the indoor and outdoor mass fractions of CO at various ambient wind speeds. The figure depicts a consistent street canyon flow field structure despite an increase in ambient wind speed, yet it promotes pollutant diffusion within the street canyon. Consequently, the concentration of indoor pollutants on the leeward side diminishes with rising ambient wind speeds. Elevated indoor pollutant concentrations on lower floors and reduced concentrations on upper floors occur with escalating ambient wind speed on the windward side. This phenomenon arises from the heightened turbulence intensity, the accelerating the transport of pollutants from the traveled way on the leeward side toward the windward side. With increasing ambient wind speed, the airflow exchange between Road 2, Road 1, and the upper part of the street canyon intensifies, leading to the removal of pollutants from the windward side out of the canyon, consequently reducing the indoor mass fraction of CO at lower levels.

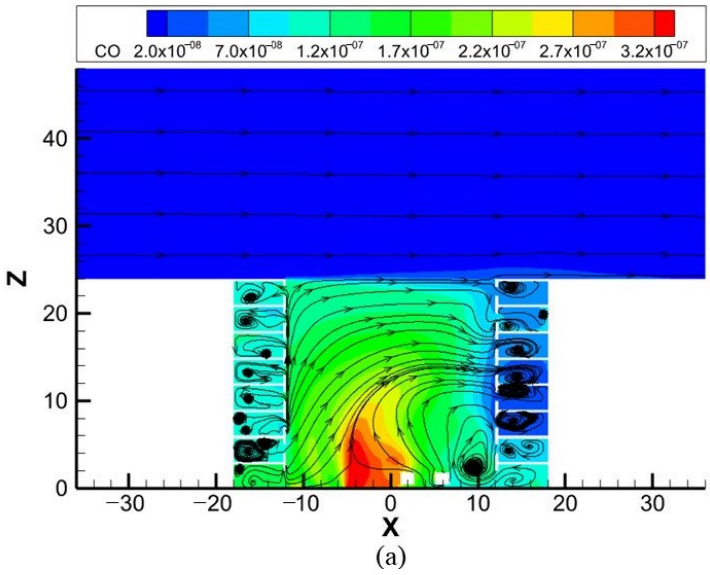

(a)

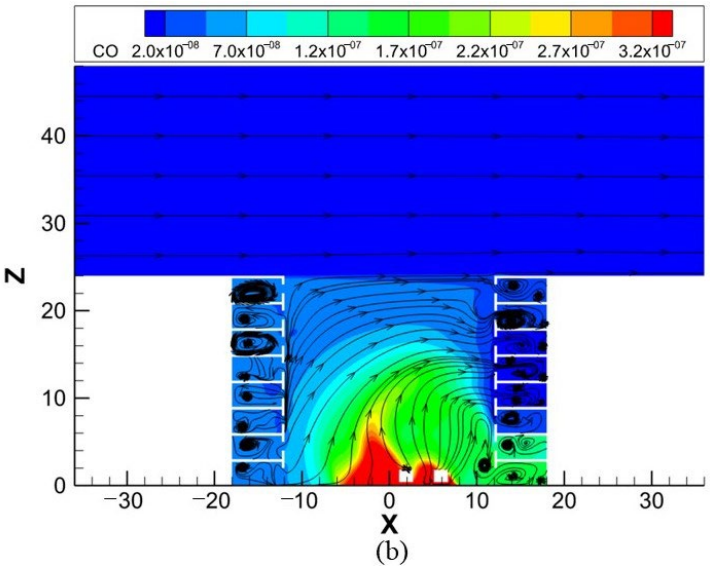

(b)

Figure 18. *Cont.*

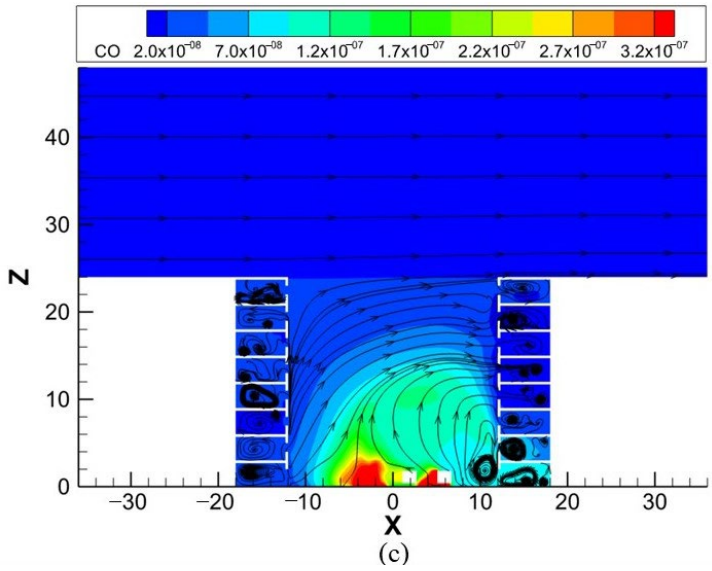

Figure 18. Indoor and outdoor mass fractions of CO at different wind speeds: (**a**) away from crossroads, (**b**) on the windward side, and (**c**) near the crossroads.

3.3. Effects of Different Aspect Ratios on Indoor–Outdoor Pollutant Coupling at Intersections

Most of the street canyon patterns are not regular, with a mix of high and low building floors. This subsection examines three distinct street canyon aspect ratios of 1/2, 1, and 2 to explore their impact on indoor and outdoor pollutant dispersion in street-facing buildings featuring windows on both adjacent walls (the data are taken from the cross-section with Y = −14.3, as shown in Figure 10). Figure 19 displays the indoor mass fraction of CO at these three distinct aspect ratios. The figure illustrates that on the windward side, an aspect ratio of H/W = 1/2 demonstrates minimal variation in pollutant concentrations across rooms, with an average mass fraction of CO of 3.54×10^{-8}. With an aspect ratio of H/W = 1, the pollutant concentrations are lower on middle floors but higher on ground and upper floors. Under H/W = 2, the indoor pollutant concentration declines with rising floors, ultimately stabilizing near 4.77×10^{-9} for the indoor mass fraction of CO. Conversely, on the leeward side, indoor pollutant concentrations exhibited a more uniform distribution across rooms, with the indoor mass fraction of CO reaching as high as 9×10^{-8} in buildings with aspect ratios of 1/2 and 1. However, with a height-to-width ratio of 2, the average indoor mass fraction of CO decreases to 2.35×10^{-8}, resulting in more uniform indoor CO concentrations across the building.

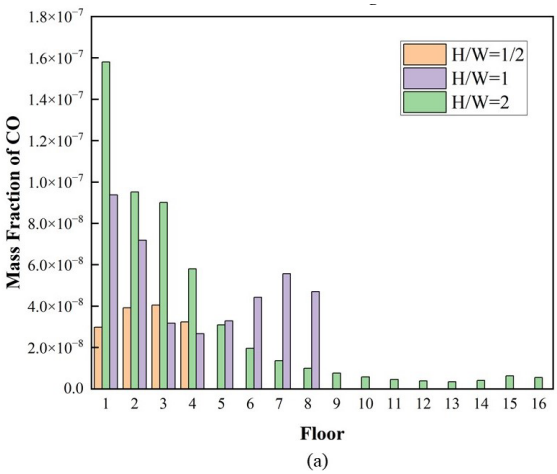

Figure 19. *Cont.*

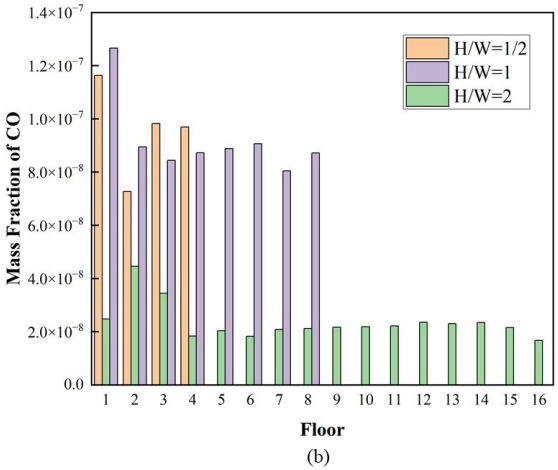

Figure 19. Indoor and outdoor pollutant mass fractions of CO for different aspect ratios: (**a**) on the leeward side, and (**b**) on the windward side.

Figure 20 depicts the indoor and outdoor mass fractions of CO distributions for three distinct aspect ratios. Observing the figure, the indoor mass fraction of CO becomes more uniform across various floors on the leeward side and diminishes as the street canyon aspect ratio increases. With an increase in the aspect ratio, alterations occur in the flow field structure on the windward side. For H/W = 1/2, the indoor mass fraction of CO exhibits minimal variation across floors due to the reduced building height. At H/W = 1, a minor vortex forms on the windward sidewalk, enhancing indoor air quality on the middle floor. Nevertheless, at H/W = 2, the street canyon's flow pattern is predominantly affected by the incoming wind from Road 1, leading to a horizontal flow between the leeward side and the windward side, resulting in decreased indoor mass fractions of CO as the floor height increases.

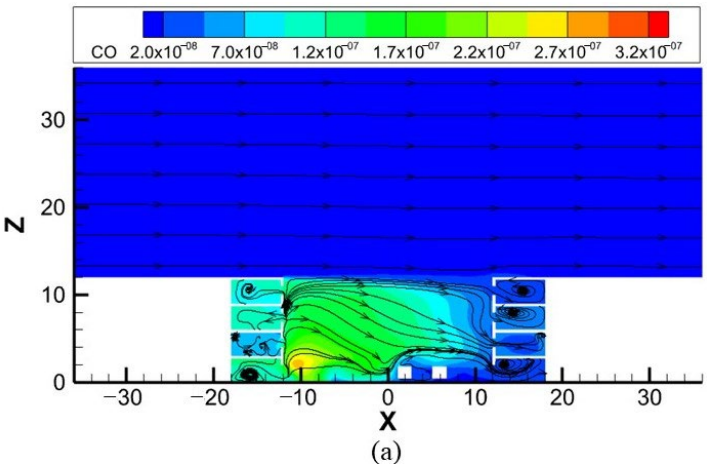

Figure 20. *Cont.*

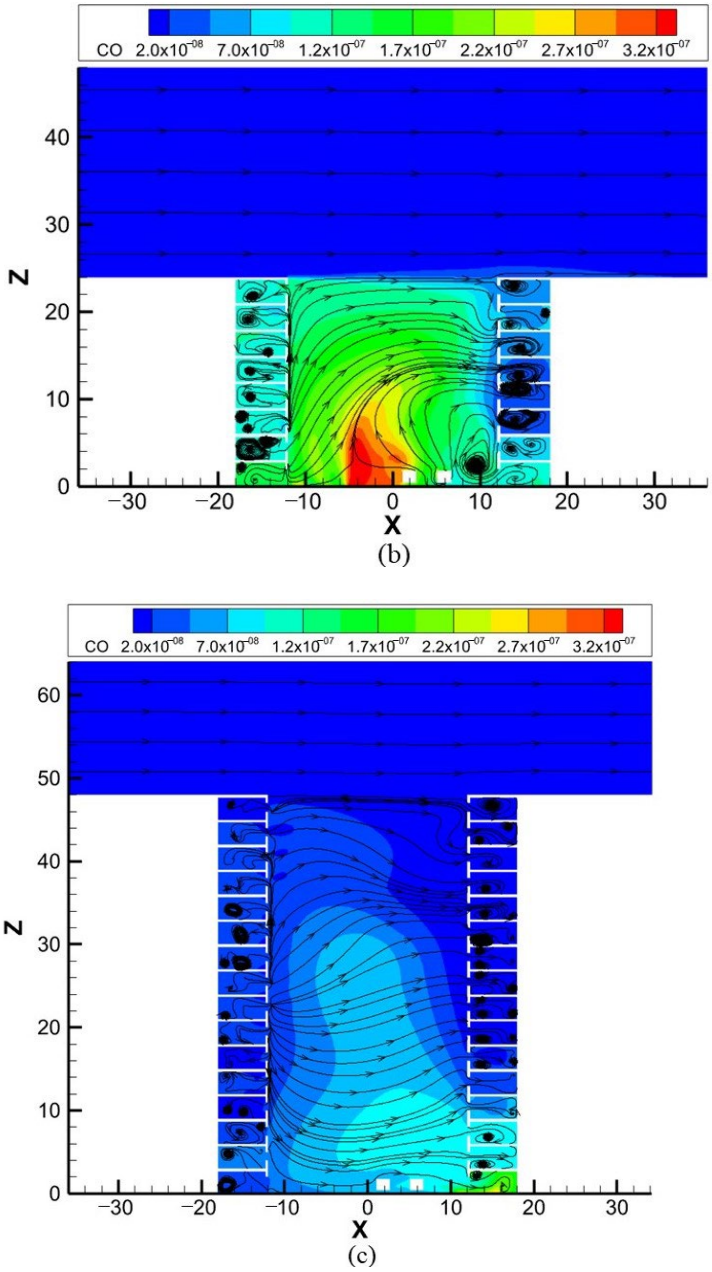

Figure 20. Indoor and outdoor mass fractions of CO for different aspect ratios: (**a**) H/W = 0.5, (**b**) H/W = 1, and (**c**) H/W = 2.

4. Discussion

This paper examines the dispersion patterns of pollutants emitted by vehicles under idling conditions at street canyon intersections. The study also explores the effects of various window opening methods on indoor air quality in street-facing buildings. The findings show that CV is effective in reducing indoor pollutant concentrations and that window-opening methods under CV significantly affect indoor pollutant levels. In addition, indoor pollutant concentrations are affected by both ambient wind speed and street canyon aspect ratios.

Current research has found that for the gas flow in intersection street canyons, the flow separation at the upstream corners of the side streets leads to the formation of vertical-axis recirculating zones at the entrances to the two side streets, which penetrate into the side streets at a distance of the order of the street width [52]. Considering the coupling of indoor and outdoor airflow, this study highlights that the airflow in the side street can flow

through rooms via windows, exchange with indoor air, and then discharge into the street canyon. This interaction has a slight impact on the gas flow in the street canyon but does not significantly alter the overall airflow pattern. Zhang et al. [53] suggest that the flow separation at upstream corners leads to the formation of vertical axis recirculating zones at the entrances to side streets, which supports our findings on airflow consistency.

Current research on building ventilation methods primarily focuses on single-sided ventilation and through ventilation. For these methods, adding one opening significantly increases the indoor ventilation rate, but beyond two openings, any further increase has a negligible impact [54]. The present study found that CV is more effective in reducing in-door pollutant concentrations compared to SSV. Specifically, CV can leverage wind direction and speed at building corners to ensure a more uniform and continuous airflow, thereby effectively reducing indoor pollutant concentrations. This finding is consistent with those of Shetabivash [55], who studied the impact of asymmetric opening positions on natural ventilation and found that corner openings can significantly enhance indoor air quality [41].

5. Conclusions

Despite the significant findings of this study on the effects of different window-opening strategies on indoor pollutant dispersion in street-facing buildings, there are several limitations that need to be addressed in future research. First, this study focused solely on carbon monoxide (CO) as the pollutant. Future research should comprehensively consider chemical reactions among various gaseous pollutants, such as $PM_{2.5}$, NO_x, and NO_2. Second, we employed a simplified vehicle model and uniform pollutant emission rates. Future studies should incorporate different vehicle shapes and displacements. Additionally, vehicle operation was not considered, and the characteristics of exhaust gas diffusion during vehicle motion were neglected. Future research could utilize dynamic mesh-updating techniques to simulate the exhaust gas emission process. Lastly, this study maintained constant indoor and outdoor temperatures. Future studies should explore the effects of solar radiation and temperature differences between indoor and outdoor environments on pollutant dispersion.

The emission of pollutants from vehicles within street canyons, coupled with insufficient ventilation inside and outside street-facing buildings, can significantly worsen indoor air quality. Following the validation of experimental data, simulations were performed to evaluate pollutant emissions from idling vehicles at intersections situated within realistic street canyons. The objective was to quantify the influence of street-facing building room window openings, room ventilation, and ambient wind speeds on flow patterns and carbon monoxide exposure within street canyons at these intersections. The following section presents the findings:

(1) Changes in the indoor flow field occurred with the change in window-opening mode. The indoor CO mass fraction was 87.1% lower in the case of optimal indoor air quality (case1.a) than in the worst case (SSV). The position of the glazing of the windows on road 1 had a greater effect on indoor pollutants than those on road 2. Comparing case 1.a, case 1.b, and case 1.c. on the windward side, the average indoor CO mass fraction for case 1.a was 4.98% and 5.22% higher than that in the other two cases when the glazing of the windows on road 2 is located away from the intersection. However, on the leeward side, the average indoor CO mass fraction in case 1.a was 64.6% and 55.1% lower compared to the other two cases.

(2) As the ambient wind speed increases, the intensity of turbulence in the street canyon increases. The mass fraction of CO decreased in the leeward-side room, increased in the ground floor room on the windward side, and decreased in the other rooms. With a higher wind speed, there is an increased exchange of airflow dynamics between the airspace over Road 2, Road 1, and the street canyon, resulting in reduced pollutant concentrations in every room. When the wind speed is 8 m/s, the average indoor CO mass fraction on the leeward side decreases to 2.45×10^{-8}.

(3) Across varying aspect ratios, the average indoor mass fraction of CO decreases on the leeward side as the aspect ratio increases, resulting in a more consistent indoor mass fraction of CO across rooms. Conversely, the indoor mass fraction of CO rises on the windward side as the aspect ratio increases. At an aspect ratio of 2, it diminishes with ascending floor levels before stabilizing around 4.77×10^{-9}. The average indoor CO mass fraction on the leeward side decreased to 2.35×10^{-8} and the indoor CO concentrations were closer on different floors.

Employing CV can effectively reduce the concentration of pollutants in the interior of a building facing a street at an intersection. Moreover, if the windows on both sides of the building are designed to be away from the intersection, CV is more effective in reducing indoor pollutant concentrations.

However, there are some aspects of our current work that require improvement, and these limitations will be further addressed in subsequent studies. Firstly, this study exclusively focuses on the dispersion characteristics of one pollutant, carbon monoxide. In future research, the chemical reactions among $PM_{2.5}$, NO_x, NO_2, and other gaseous pollutants should be comprehensively considered. Secondly, a simplified approach was used to set the mass fraction of carbon monoxide emitted by all types of vehicles uniformly. Future studies should incorporate different vehicle shapes and displacements. Additionally, vehicle operation was not taken into account, and the diffusion characteristics of exhaust gas while the vehicle is in motion were neglected. Future research could utilize the dynamic mesh-updating technique to simulate the exhaust gas emission process. Lastly, this study maintained consistent and unchanging indoor and outdoor temperatures. Future studies should explore the effects of solar radiation and temperature differences between indoor and outdoor environments on pollutant diffusion.

Author Contributions: Conceptualization, Y.W. and Y.O.; methodology, T.S. and T.M.; software, Y.O.; validation, Z.L. and T.S.; formal analysis, Y.W.; investigation, Y.W.; resources, Y.W.; data curation, Z.L.; writing—original draft preparation, Y.O.; writing—review and editing, T.S.; visualization, Y.W.; supervision, T.M.; project administration, T.M.; funding acquisition, Y.W. All authors have read and agreed to the published version of the manuscript.

Funding: This research was supported by the National Natural Science Foundation of China (Grant No. 52278123), CITIC General Institute of Architectural Design and Research (No. 2022ZXKYD30100), and the Scientific Research Foundation of the Wuhan University of Technology (Grant No. 40120237 and 40120551).

Institutional Review Board Statement: Not applicable.

Informed Consent Statement: Not applicable.

Data Availability Statement: The data presented in this study are available through email upon request to the corresponding author. The data are not publicly available due to privacy.

Acknowledgments: The authors extend their deepest gratitude to Yanhua Chen, Chief Engineer at CITIC General Institute of Architectural Design and Research Co., Ltd., for his invaluable guidance and contributions to the conceptual development and formulation of the ideas presented in this paper. His expertise and support have been instrumental in shaping the research and enhancing the overall quality of the work.

Conflicts of Interest: Tianhao Shi is an employee of CITIC General Institute of Architectural Design and Research Co., Ltd. The paper reflects the views of the scientists and not the company.

Nomenclature

ρ	Air density	ν	Kinematic viscosity
P	Air pressure	δ_{ij}	Kronecker delta
$u'_i u'_j$	Reynolds stress term	C	Pollutant concentration
S_c	Pollutant emission rate	K_c	Turbulent diffusion coefficient of pollutants
U_{ref}	Wind velocity at the reference height	z_{ref}	Reference height
α	Ground roughness index	U^*	Friction velocity

References

1. Luo, H.; Han, Y.; Cheng, X.; Lu, C.; Wu, Y. Spatiotemporal variations in particulate matter and air quality over China: National, regional and urban scales. *Atmosphere* **2020**, *12*, 43. [CrossRef]
2. Liang, M.; Chao, Y.; Tu, Y.; Xu, T. Vehicle Pollutant Dispersion in the Urban Atmospheric Environment: A Review of Mechanism, Modeling, and Application. *Atmosphere* **2023**, *14*, 279. [CrossRef]
3. Van Hooff, T.; Blocken, B. On the effect of wind direction and urban surroundings on natural ventilation of a large semi-enclosed stadium. *Comput. Fluids* **2010**, *39*, 1146–1155. [CrossRef]
4. Ai, Z.; Mak, C.M. From street canyon microclimate to indoor environmental quality in naturally ventilated urban buildings: Issues and possibilities for improvement. *Build. Environ.* **2015**, *94*, 489–503. [CrossRef] [PubMed]
5. Hu, Y.; Wu, Y.; Wang, Q.; Hang, J.; Li, Q.; Liang, J.; Ling, H.; Zhang, X. Impact of indoor-outdoor temperature difference on building ventilation and pollutant dispersion within urban communities. *Atmosphere* **2021**, *13*, 28. [CrossRef]
6. Nguyen, V.T.; Nguyen, T.C.; Nguyen, J. Numerical simulation of turbulent flow and pollutant dispersion in urban street canyons. *Atmosphere* **2019**, *10*, 683. [CrossRef]
7. Liu, F.; Qian, H.; Zheng, X.; Zhang, L.; Liang, W. Numerical study on the urban ventilation in regulating microclimate and pollutant dispersion in urban street canyon: A case study of Nanjing new region, China. *Atmosphere* **2017**, *8*, 164. [CrossRef]
8. Santiago, J.-L.; Sanchez, B.; Rivas, E.; Vivanco, M.G.; Theobald, M.R.; Garrido, J.L.; Gil, V.; Martilli, A.; Rodríguez-Sánchez, A.; Buccolieri, R. High spatial resolution assessment of the effect of the Spanish National Air Pollution Control Programme on street-level NO_2 concentrations in three neighborhoods of Madrid (Spain) using mesoscale and CFD modelling. *Atmosphere* **2022**, *13*, 248. [CrossRef]
9. Linda, J.; Pospíšil, J.; Köbölová, K. Identification of Wind-Induced Particle Resuspension in Urban Environment Using CFD Modelling. *Atmosphere* **2022**, *14*, 57. [CrossRef]
10. Ho, Y.-K.; Liu, C.-H. Street-level ventilation in hypothetical urban areas. *Atmosphere* **2017**, *8*, 124. [CrossRef]
11. Chew, L.W.; Nazarian, N.; Norford, L. Pedestrian-level urban wind flow enhancement with wind catchers. *Atmosphere* **2017**, *8*, 159. [CrossRef]
12. Schalau, S.; Habib, A.; Michel, S. A modified k-ε turbulence model for heavy gas dispersion in built-up environment. *Atmosphere* **2023**, *14*, 161. [CrossRef]
13. Rakowska, A.; Wong, K.C.; Townsend, T.; Chan, K.L.; Westerdahl, D.; Ng, S.; Močnik, G.; Drinovec, L.; Ning, Z. Impact of traffic volume and composition on the air quality and pedestrian exposure in urban street canyon. *Atmos. Environ.* **2014**, *98*, 260–270. [CrossRef]
14. Kwak, K.-H.; Woo, S.H.; Kim, K.H.; Lee, S.-B.; Bae, G.-N.; Ma, Y.-I.; Sunwoo, Y.; Baik, J.-J. On-road air quality associated with traffic composition and street-canyon ventilation: Mobile monitoring and CFD modeling. *Atmosphere* **2018**, *9*, 92. [CrossRef]
15. Joubert, L.; Leroy, G.; Claude, T.; Riahi, O. Experimental Campaign of Massive CO_2 Atmospheric Releases in an Urban Area. *Atmosphere* **2023**, *14*, 1428. [CrossRef]
16. Tong, H.; Hung, W.; Cheung, C.S. Development of a driving cycle for Hong Kong. *Atmos. Environ.* **1999**, *33*, 2323–2335. [CrossRef]
17. Ahmad, K.; Khare, M.; Chaudhry, K. Model vehicle movement system in wind tunnels for exhaust dispersion studies under various urban street configurations. *J. Wind Eng. Ind. Aerodyn.* **2002**, *90*, 1051–1064. [CrossRef]
18. Ning, Z.; Cheung, C.S.; Lu, Y.; Liu, M.; Hung, W. Experimental and numerical study of the dispersion of motor vehicle pollutants under idle condition. *Atmos. Environ.* **2005**, *39*, 7880–7893. [CrossRef]
19. He, B.-J.; Ding, L.; Prasad, D. Enhancing urban ventilation performance through the development of precinct ventilation zones: A case study based on the Greater Sydney, Australia. *Sustain. Cities Soc.* **2019**, *47*, 101472. [CrossRef]
20. Achour-Younsi, S.; Kharrat, F. Outdoor thermal comfort: Impact of the geometry of an urban street canyon in a Mediterranean subtropical climate–case study Tunis, Tunisia. *Procedia-Soc. Behav. Sci.* **2016**, *216*, 689–700. [CrossRef]
21. Shishegar, N. Street design and urban microclimate: Analyzing the effects of street geometryand orientation on airflow and solar access in urban canyons. *J. Clean Energy Technol.* **2013**, *1*, 52–56. [CrossRef]
22. Hang, J.; Buccolieri, R.; Yang, X.; Yang, H.; Quarta, F.; Wang, B. Impact of indoor-outdoor temperature differences on dispersion of gaseous pollutant and particles in idealized street canyons with and without viaduct settings. In *Building Simulation*; Tsinghua University Press: Beijing, China, 2019; pp. 285–297.
23. Ding, S.; Huang, Y.; Cui, P.; Wu, J.; Li, M.; Liu, D. Impact of viaduct on flow reversion and pollutant dispersion in 2D urban street canyon with different roof shapes-Numerical simulation and wind tunnel experiment. *Sci. Total Environ.* **2019**, *671*, 976–991. [CrossRef]

24. Ming, T.; Nie, C.; Li, W.; Kang, X.; Wu, Y.; Zhang, M.; Peng, C. Numerical study of reactive pollutants diffusion in urban street canyons with a viaduct. In *Building Simulation*; Tsinghua University Press: Beijing, China, 2022; pp. 1227–1241.
25. Ming, T.; Han, H.; Zhao, Z.; de Richter, R.; Wu, Y.; Li, W.; Wong, N.H. Field synergy analysis of pollutant dispersion in street canyons and its optimization by adding wind catchers. In *Building Simulation*; Tsinghua University Press: Beijing, China, 2021; pp. 391–405.
26. Montazeri, H.; Montazeri, F. CFD simulation of cross-ventilation in buildings using rooftop wind-catchers: Impact of outlet openings. *Renew. Energy* **2018**, *118*, 502–520. [CrossRef]
27. Zhang, K.; Chen, G.; Wang, X.; Liu, S.; Mak, C.M.; Fan, Y.; Hang, J. Numerical evaluations of urban design technique to reduce vehicular personal intake fraction in deep street canyons. *Sci. Total Environ.* **2019**, *653*, 968–994. [CrossRef] [PubMed]
28. Gromke, C.; Ruck, B. Pollutant concentrations in street canyons of different aspect ratio with avenues of trees for various wind directions. *Bound. -Layer Meteorol.* **2012**, *144*, 41–64. [CrossRef]
29. Gromke, C.; Buccolieri, R.; Di Sabatino, S.; Ruck, B. Dispersion study in a street canyon with tree planting by means of wind tunnel and numerical investigations–evaluation of CFD data with experimental data. *Atmos. Environ.* **2008**, *42*, 8640–8650. [CrossRef]
30. Lin, Y.; Chen, G.; Chen, T.; Luo, Z.; Yuan, C.; Gao, P.; Hang, J. The influence of advertisement boards, street and source layouts on CO dispersion and building intake fraction in three-dimensional urban-like models. *Build. Environ.* **2019**, *150*, 297–321. [CrossRef]
31. Li, Z.; Zhang, H.; Wen, C.-Y.; Yang, A.-S.; Juan, Y.-H. Effects of height-asymmetric street canyon configurations on outdoor air temperature and air quality. *Build. Environ.* **2020**, *183*, 107195. [CrossRef]
32. Liu, J.; Cui, S.; Chen, G.; Zhang, Y.; Wang, X.; Wang, Q.; Gao, P.; Hang, J. The influence of solar natural heating and NOx-O3 photochemistry on flow and reactive pollutant exposure in 2D street canyons. *Sci. Total Environ.* **2021**, *759*, 143527. [CrossRef] [PubMed]
33. Xie, X.; Huang, Z.; Wang, J.; Xie, Z. The impact of solar radiation and street layout on pollutant dispersion in street canyon. *Build. Environ.* **2005**, *40*, 201–212. [CrossRef]
34. Guo, X.; Buccolieri, R.; Gao, Z.; Zhang, M.; Lyu, T.; Rui, L.; Shen, J. On the effects of urban-like intersections on ventilation and pollutant dispersion. In *Building Simulation*; Tsinghua University Press: Beijing, China, 2022; pp. 419–433.
35. Scaperdas, A.; Colvile, R. Assessing the representativeness of monitoring data from an urban intersection site in central London, UK. *Atmos. Environ.* **1999**, *33*, 661–674. [CrossRef]
36. Li, M.; Gernand, J.M. Identifying shelter locations and building air intake risk from release of particulate matter in a three-dimensional street canyon via wind tunnel and CFD simulation. *Air Qual. Atmos. Health* **2019**, *12*, 1387–1398. [CrossRef]
37. Hassan, S.; Akter, U.H.; Nag, P.; Molla, M.M.; Khan, A.; Hasan, M.F. Large-Eddy simulation of airflow and pollutant dispersion in a model street canyon intersection of Dhaka city. *Atmosphere* **2022**, *13*, 1028. [CrossRef]
38. He, Y.; Tablada, A.; Wong, N.H. A parametric study of angular road patterns on pedestrian ventilation in high-density urban areas. *Build. Environ.* **2019**, *151*, 251–267. [CrossRef]
39. Yang, F.; Kang, Y.; Gao, Y.; Zhong, K. Numerical simulations of the effect of outdoor pollutants on indoor air quality of buildings next to a street canyon. *Build. Environ.* **2015**, *87*, 10–22. [CrossRef]
40. Gao, C.; Lee, W.L. Evaluating the influence of window types on the natural ventilation performance of residential buildings in Hong Kong. *Int. J. Vent.* **2011**, *10*, 227–238. [CrossRef]
41. Perén, J.; Van Hooff, T.; Leite, B.C.C.; Blocken, B. CFD analysis of cross-ventilation of a generic isolated building with asymmetric opening positions: Impact of roof angle and opening location. *Build. Environ.* **2015**, *85*, 263–276. [CrossRef]
42. Prakash, D.; Ravikumar, P. Analysis of thermal comfort and indoor air flow characteristics for a residential building room under generalized window opening position at the adjacent walls. *Int. J. Sustain. Built Environ.* **2015**, *4*, 42–57. [CrossRef]
43. Hang, J.; Luo, Z.; Wang, X.; He, L.; Wang, B.; Zhu, W. The influence of street layouts and viaduct settings on daily carbon monoxide exposure and intake fraction in idealized urban canyons. *Environ. Pollut.* **2017**, *220*, 72–86. [CrossRef] [PubMed]
44. Hang, J.; Li, Y.; Sandberg, M.; Buccolieri, R.; Di Sabatino, S. The influence of building height variability on pollutant dispersion and pedestrian ventilation in idealized high-rise urban areas. *Build. Environ.* **2012**, *56*, 346–360. [CrossRef]
45. Wang, H.; Chen, Q. A new empirical model for predicting single-sided, wind-driven natural ventilation in buildings. *Energy Build.* **2012**, *54*, 386–394. [CrossRef]
46. Tominaga, Y.; Mochida, A.; Yoshie, R.; Kataoka, H.; Nozu, T.; Yoshikawa, M.; Shirasawa, T. AIJ guidelines for practical applications of CFD to pedestrian wind environment around buildings. *J. Wind Eng. Ind. Aerodyn.* **2008**, *96*, 1749–1761. [CrossRef]
47. Cui, P.-Y.; Li, Z.; Tao, W.-Q. Investigation of Re-independence of turbulent flow and pollutant dispersion in urban street canyon using numerical wind tunnel (NWT) models. *Int. J. Heat Mass Transf.* **2014**, *79*, 176–188. [CrossRef]
48. Janour, Z.; Jurcakova, K.; Brych, K.; Dittrt, F.; Dittrich, F. Potential risks at an industrial site: A wind tunnel study. *Process Saf. Environ. Prot.* **2010**, *88*, 185–190. [CrossRef]
49. Yassin, M.F.; Kellnerova, R.; Jaňour, Z. Impact of street intersections on air quality in an urban environment. *Atmos. Environ.* **2008**, *42*, 4948–4963. [CrossRef]
50. Meroney, R.N.; Pavageau, M.; Rafailidis, S.; Schatzmann, M. Study of line source characteristics for 2-D physical modelling of pollutant dispersion in street canyons. *J. Wind Eng. Ind. Aerodyn.* **1996**, *62*, 37–56. [CrossRef]
51. Jiang, Y.; Alexander, D.; Jenkins, H.; Arthur, R.; Chen, Q. Natural ventilation in buildings: Measurement in a wind tunnel and numerical simulation with large-eddy simulation. *J. Wind Eng. Ind. Aerodyn.* **2003**, *91*, 331–353. [CrossRef]

52. Soulhac, L.; Garbero, V.; Salizzoni, P.; Mejean, P.; Perkins, R. Flow and dispersion in street intersections. *Atmos. Environ.* **2009**, *43*, 2981–2996. [CrossRef]
53. Zhang, H.; Xu, T.; Wang, Y.; Zong, Y.; Li, S.; Tang, H. Study on the influence of meteorological conditions and the street side buildings on the pollutant dispersion in the street canyon. In *Building Simulation*; Tsinghua University Press: Beijing, China, 2016; pp. 717–727.
54. Zhang, X.; Weerasuriya, A.U.; Wang, J.; Li, C.Y.; Chen, Z.; Tse, K.T.; Hang, J. Cross-ventilation of a generic building with various configurations of external and internal openings. *Build. Environ.* **2022**, *207*, 108447. [CrossRef]
55. Shetabivash, H. Investigation of opening position and shape on the natural cross ventilation. *Energy Build.* **2015**, *93*, 1–15. [CrossRef]

Disclaimer/Publisher's Note: The statements, opinions and data contained in all publications are solely those of the individual author(s) and contributor(s) and not of MDPI and/or the editor(s). MDPI and/or the editor(s) disclaim responsibility for any injury to people or property resulting from any ideas, methods, instructions or products referred to in the content.